PNAS
www.pnas.org

Supplementary Information for

Human cGAS has an additional DNA-binding interface that enhances enzymatic activity and liquid phase condensation

Wei Xie[1,*], Lodoe Lama[2], Carolina Adura[3], Daisuke Tomita[4], J. Fraser Glickman[3], Thomas Tuschl[2] and Dinshaw J. Patel[1,*]

*Correspondence: D.J.P. (pateld@mskcc.org); W.X. (xiew@mskcc.org)

This PDF file includes:

www.pnas.org/cgi/doi/10.1073/pnas.1905013116

SI Materials and Methods

Protein expression and purification. The SRY.h-cGAS^{CD} construct was designed to contain the first HMG box of human SRY (1-87) replacing the N-terminal domain h-cGAS domain together with h-cGAS^{CD} (160-522). The sequence corresponding to SRY.h-cGAS^{CD} was synthesized by Integrated DNA Technologies (IDT) and cloned into a pRSFDuet-1 vector (Novagen) engineered with an N-terminal hexa-histidine (His_6)-SUMO tag. The fusion protein was expressed in *Escherichia coli* strain BL21-CodonPlus(DE3)-RIL (Stratagene). Bacteria were grown in Luria-Bertani (LB) medium supplemented with 50 mg/ml kanamycin at 37°C to OD_{600} of 0.8, and induced by 0.3 mM isopropyl β-D-1-thiogalactopyranoside (IPTG) at 18°C overnight. Bacteria cells were harvested by centrifugation at 4°C and lysed by the EmulsiFlex-C3 homogenizer (Avestin) in buffer A (500 mM NaCl, 20 mM imidazole, and 50 mM Tris-HCl, pH 8.0) supplemented with 1 mM phenylmethylsulfonyl fluoride (PMSF) protease inhibitor and 0.5% Triton X-100. Cell lysates were centrifuged at 20,000 r.p.m for 0.5 h in a JA-20 fixed angle rotor (Avanti J-E series centrifuge, Beckman Coulter). The supernatant was loaded onto a 5 mL HisTrap FF column (GE Healthcare), and followed by extensive washing with buffer A. The target protein was eluted with buffer A supplemented with 400 mM imidazole. The eluted protein was incubated with ubiquitin-like protease (ULP1) during dialysis at 4°C overnight against buffer B containing 20 mM Tris-HCl, pH 7.5, 20 mM imidazole, 300 mM NaCl, 1 mM $MgCl_2$, and 5 mM β-mercaptoethanol. The SUMO-tags were removed by reloading on HisTrap FF column. The flow-through was further loaded on 5 mL HiTrap Heparin column (GE Healthcare) pre-equilibrated in buffer B. Elution of recombinant proteins was achieved by a linear gradient from 300 mM to 1 M NaCl in 15 column volumes. The fractions were monitored by SDS-PAGE, and the target proteins were concentrated by Amicon concentrators and loaded on Superdex 200 16/60 column pre-equilibrated in buffer C (20 mM Tris-HCl, pH 7.5, 300 mM NaCl, 2 mM $MgCl_2$ and 1 mM DTT). The high purity eluting fractions were detected by SDS-PAGE and concentrated to around 10 mg/ml. The protein was flash-frozen in liquid nitrogen and stored at -80°C.

The engineered pRSFDuet-1 plasmids to express His_6-SUMO tagged h-cGAS (1-522), h-cGAS^{CD} (160-522), m-cGAS (1-507) and m-cGAS^{CD} (147-507) were stocked in our group. All mutants were generated by site-directed mutagenesis with a QuikChange II XL kit (Agilent) according to the manufacturer's instruction and confirmed by sequencing. The expression and purification of these proteins were the same as that for SRY.h-cGAS^{CD}.

Crystallization. Synthetic DNA oligonucleotides (IDT) were dissolved and mixed in water, followed by annealing according to the manufacturer's instructions.

Crystallization conditions were determined with crystal screens (Qiagen) by sitting-drop vapor diffusion with a Mosquito crystallization robot (TTP Labtech). Crystallization conditions were optimized using the hanging drop vapor diffusion method at 20°C. SRY.h-cGAS^{CD}-DNA binary complex samples were prepared by mixing SRY.h-cGAS^{CD} protein with 21-bp DNA (containing 1-nt 5′-overhang at either end: upper strand sequence: 5′-CGATCCGGGATCTAAACAATGC-3′; lower strand sequence: 5′-GGCATTGTTTAGATCCCGGATC-3′) in a 1:1.2 molar ratio in buffer C (20 mM Tris-HCl, pH 7.5, 300 mM NaCl, 1 mM DTT, and 2 mM $MgCl_2$) and incubated on ice for 1h. The crystals were grown from drops mixed from 1.5 µL of SRY.h-cGAS^{CD}-DNA solution (about 4 mg/ml protein) and 1.5 µL of reservoir solution (0.2 M L-proline, 0.1 M HEPES, pH 7.5, 8% PEG3350 (v/v), 10 mM $MgCl_2$).

To assemble the h-cGAS^{CD}-DNA binary complex, the purified K299E/R300A/K301E triple mutant h-cGAS^{CD} (152-522) protein was mixed with the 16-bp DNA (containing 1-nt 5′-overhang at either end: upper strand sequence: 5′- AAATTGCCGAAGACGAA-3′; lower strand sequence 5′-TTTCGTCTTCGGCAATT-3′) at the molar ratio of 1:1.2 in buffer 200 (20 mM Tris-HCl, pH 7.5, 200 mM NaCl, 1 mM DTT, and 2 mM $MgCl_2$) and incubated on ice for 1h. Crystals were grown from drops consisting of 1 µL protein solution (about 5 mg/ml) and 1 µL reservoir solution containing 0.2 M NaCl, 0.1 M HEPES, pH 7.5, and 28% PEG400 (v/v).

To obtain the structure of the h-cGAS^{CD}-RU.521 complex, we generated the K427E/K428E dual mutant h-cGAS^{CD}(152-522). Protein crystals were grown in drops mixed from 1 µl of protein solution (about 8 mg/ml in buffer 20 mM Tris-HCl, pH 7.5, 300 mM NaCl, 1 mM DTT, and 2 mM $MgCl_2$) and 1 µl of reservoir solution (0.064 M sodium citrate 7.0, 0.1 M HEPES, pH 7.0, 10% PEG5000MME) at 20°C. The crystals were soaked in the reservoir solution containing 20 mM RU.521 and 20% DMSO for 4h.

For data collection, crystals were cryoprotected in reservoir solution supplemented with 30% glycerol and flash frozen in liquid nitrogen.

Structure determination. All the diffraction data sets were collected on the 24-ID beamline at the Advanced Photon Source (APS) at the Argonne National Laboratory. The diffraction data of SRY.h-cGAS^{CD}-DNA binary complex and the complex of RU.521 bound to apo h-cGAS^{CD} was indexed, integrated and scaled with the HKL2000 program. The diffraction data of mutated h-cGAS^{CD}-DNA binary complex were auto-processed by the NECAT RAPD online server. The structure of the SRY.h-cGAS^{CD}-DNA complex was solved by molecular replacement method with program PHASER(1) of the PHENIX package(2), using the modified m-cGAS^{CD}-DNA structure (RCSB code: 4K96) and SRY-DNA structure (PDB code:

2GZK) as the search model. The structure of the mutated h-cGAS^{CD}-DNA binary complex was solved by molecular replacement using modified m-cGAS^{CD}-DNA structure (RCSB code: 4K96) as the search model. The h-cGAS^{CD}-RU.521 complex structure was solved by molecular replacement using apo h-cGAS^{CD} structure (RCSB code: 4O68) as the search model. The initial maps showed clear density for most regions of the protein-DNA complexes. Iterative manual model building was performed using the program COOT (3), and refinement with phenix.refine produced the final models of the complexes(4). The statistics of the data collection and refinement are shown in Supplementary Tables 1 and 2. Figures were generated using PyMOL (http://www.pymol.org).

SEC-MALS experiments. For protein molar mass determination, purified cGAS proteins were analyzed using an ÄKTA-MALS system. A miniDAWN TREOS multi-angle light scattering detector (Wyatt Technology) and an Optilab T-rEX refractometer (Wyatt Technology) were used in-line with Superdex 200 Increase 10/300 gel filtration column (GE Healthcare) pre-equilibrated in buffer 20 mM Tris 7.5, 1 mM DTT, and 300 mM NaCl at a flow rate of 0.3 mL/min. Separation and ultraviolet detection were performed by ÄKTA Pure system (GE Healthcare), light scattering was monitored by miniDAWN TREOS system, and concentration was measured by the Optilab T-rEX differential refractometer. Molar masses of proteins were calculated using the Astra 6.1 program (Wyatt Technology) with a dn/dc value of 0.185 mL/g.

Rapid-Fire 365 mass spectrometry (RF-MS) validation assay. Enzymatic activities of h-cGAS and m-cGAS enzymes were detected using RapidFire 365 mass spectrometry (RF-MS) similar to the method described previously for m-cGAS(5). Briefly, for m-cGAS, each reaction contained 300 nM dsDNA ligand of indicated length, 60 nM full-length cGAS proteins and 300 μM ATP/GTP in 20 μL final reaction volume. The samples were incubated at 37˚C for 1 h and stopped by addition of 60 μL of 0.5% (v/v) formic acid per well followed by RF-MS analysis as described previously. To measure enzymatic activities of h-cGAS and mutants, each reaction sample contained 25 nM of 100-bp dsDNA, 100 nM cGAS proteins and 100 μM ATP/GTP. The samples were incubated at room temperature (RT) or 37˚C for the indicated time period followed by addition of 60 μL of 0.5% (v/v) formic acid per well to stop the reaction.
DNA oligonucleotides were designed based on previous report (6), and obtained from IDT. DNA oligonucleotides were dissolved and hybridized in water, followed by annealing according to the manufacturer's instructions.
100-bp Forward sequence:

5′-
ACATCTAGTACATGTCTAGTCAGTATCTAGTGATTATCTAGACATACATCTAG
-TACATGTCTAGTCAGTATCTAGTGATTATCTAGACATGGACTCATCC-3′
100-bp Reverse sequence:
5′-
GGATGAGTCCATGTCTAGATAATCACTAGATACTGACTAGACATGTACTAGA
T-GTATGTCTAGATAATCACTAGATACTGACTAGACATGTACTAGATGT-3′
45-bp Forward sequence:
5′- TACAGATCTACTAGTGATCTATGACTGATCTGTACATGATCTACA-3′
45-bp Reverse sequence:
5′-TGTAGATCATGTACAGATCAGTCATAGATCACTAGTAGATCTGTA-3′
25-bp Forward sequence:
5′-TACAGATCTACTAGTGATCTATGAC-3′
25-bp Reverse sequence:
5′-GTCATAGATCACTAGTAGATCTGTA-3′

Electrophoretic mobility shift assay. Recombinant cGAS proteins and Cy3 labeled ISD45 DNA were incubated at room temperature for 30 min in buffer (20 mM Hepes, pH 7.2, 150 mM NaCl,) for sample volume of 10 μL. The binding reactions contained 1 pmol Cy3-ISD45 and cGAS proteins ranged from 1 pmol to 32 pmol with 2-fold increase. After reaction, 5 μL 3× native DNA loading buffer (20 mM Hepes, pH 7.2, 150 mM NaCl, 30% Sucrose, 0.01% Bromophenol Blue) was added. Reactions were detected by electrophoresis at 4˚C on 12 wells 6% DNA retardation gels (Invitrogen) in 0.5× TBE buffer. Gels were scanned using the Typhoon FLA-9500 imager (GE healthcare) and visualized using FIJI/ImageJ.

DNA condensation assay. Recombinant cGAS proteins and Cy3 labeled ISD100 DNA were incubated at room temperature for 1h in buffer (20 mM Hepes, pH 7.2, 150 mM NaCl). Each reaction contained 1 pmol Cy3-ISD100. cGAS proteins were added from 0.25 pmol to 16 pmol with 2-fold increase for a final sample volume of 25 μL. After incubation, mixtures were centrifuged at 13,000 g for 5 min. 20 μL Supernatant was transferred to a Greiner 384 wells plate. The Cy3 fluorescence intensity of each supernatant was quantified on the TECAN infinite M1000 plate reader using 550 ± 5 nm excitation and 570 ± 5 nm emission wavelengths. The fluorescence intensity values of Cy3 in the supernatant were plotted against cGAS protein concentrations using GraphPad Prism 7. Data are represented as means ± SD of three independent experiments.

Turbidity measurements. Wild-type human cGAS or variants were diluted to 10 μM in the buffer (20 mM Tris, pH 7.5 with 100 mM, 200 mM, 300 mM, or 500 mM

NaCl). Phase separation was initiated by addition of 10 μM ISD100 in a 40 μL final volume in a Greiner 384 well transparent microplate, and turbidity was detected after incubation for 0.5 hours at room temperature by absorbance of 350 nm wavelength light using a TECAN infinite M1000 microplate reader. The absorbance values were plotted against NaCl concentrations using GraphPad Prism 7. Data are represented as means ± SD of three independent experiments.

Time lapse imaging of liquid droplet formation measurements. Recombinant FL WT h-cGAS proteins were labeled using Alexa Fluor 488 protein labeling kit (Invitrogen) according to manufacturer's instructions. DNA-induced cGAS phase separation assay was performed as previously reported (7). 10 μM FL WT-h-cGAS protein (5% Alexa Fluor 488 protein labeled in buffer 20 mM Tris-HCl, pH 7.5, 300 mM NaCl, 1 mg/ml BSA) was mixed with 10 μM ISD100 in 96-well plates (Falcon) pre-coated with 10 mg/ml BSA (Sigma) to a final volume of 50 μL. Avoid mixing the protein and DNA by pipetting up and down. The same protocol was used for unlabeled h-cGAS and m-cGAS mutation proteins. The time-lapse experiment was conducted on AxioObserver Z1 (Carl Zeiss) using 40x/0.6NA objective and Hamamatsu Flash4.0 cMOS camera. Bright-field and GFP channels were imaged every 5 min for 2 h. The time-lapse data were processed using FIJI/ImageJ.

References

1. McCoy AJ, et al. (2007) Phaser crystallographic software. *J Appl Crystallogr* 40:658–674.
2. Adams PD, et al. (2010) PHENIX: A comprehensive Python-based system for macromolecular structure solution. *Acta Crystallogr Sect D Biol Crystallogr* 66:213–221.
3. Emsley P, Lohkamp B, Scott WG, Cowtan K (2010) Features and development of Coot. *Acta Crystallogr Sect D Biol Crystallogr* 66:486–501.
4. Afonine P V, et al. (2012) Towards automated crystallographic structure refinement with phenix.refine. *Acta Crystallogr D Biol Crystallogr* 68:352–367.
5. Vincent J, et al. (2017) Small molecule inhibition of cGAS reduces interferon expression in primary macrophages from autoimmune mice. *Nat Commun* 8:750.
6. An J, Woodward JJ, Sasaki T, Minie M, Elkon KB (2015) Cutting Edge: Antimalarial Drugs Inhibit IFN-β Production through Blockade of Cyclic GMP-AMP Synthase–DNA Interaction. *J Immunol* 194:4089–4093.
7. Du M, Chen ZJ (2018) DNA-induced liquid phase condensation of cGAS activates innate immune signaling. *Science* 361:704–709.

SUPPLEMENTARY FIGURES

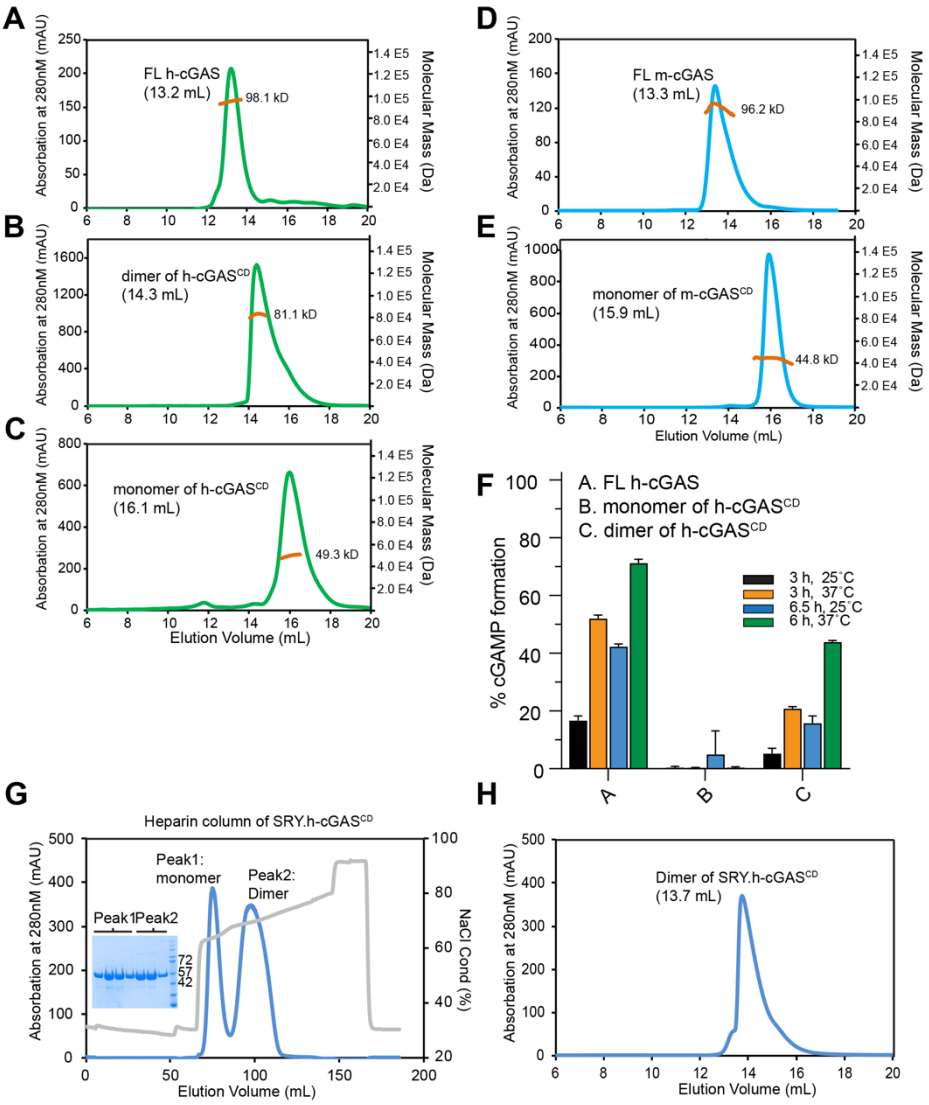

Fig. S1. N-terminal domain of cGAS promotes DNA-free cGAS dimerization. (*A-E*) SEC-MALS detection of oligomeric states of DNA-free cGAS proteins in solution. The horizontal orange line represents the calculated molecular mass for cGAS. The elution time and molecular mass are indicated in the panels. The calculated mol wt of the hcGAS^{CD} dimer is less than two-fold of the molecular weight of the monomer. It is conceivable that this discrepancy in the expected mol wt of the hcGAS^{CD} dimer reflects a dimer-monomer equilibrium, with the tailing peak in panel B, consistent with a monomer component. In addition, the very small difference of the elution volume (16.1 ml in panel C and 15.9 ml in panel E) could arise from potentially slightly different three-dimensional shapes of human and mouse cGAS^{CD}. (*F*) Enzymatic activity of FL h-cGAS and h-cGAS^{CD}, detected by RF-MS assay. Purified dimers and monomers of h-cGAS^{CD} were tested respectively. The varying incubation time and temperature are indicated by different colors. Data are

represented as means ± SD of three independent experiments. (*G*) SRY.h-cGAS^{CD} eluted as both monomer and dimer peaks during heparin column purification. Both peaks eluted with high concentration of salt, indicating high DNA binding affinity. (*H*) The peak of SRY.h-cGAS^{CD} eluting from heparin column with higher salt concentration was shown to be dimer (13.7 mL) in Gel filtration (Superdex 200 16/60 column).

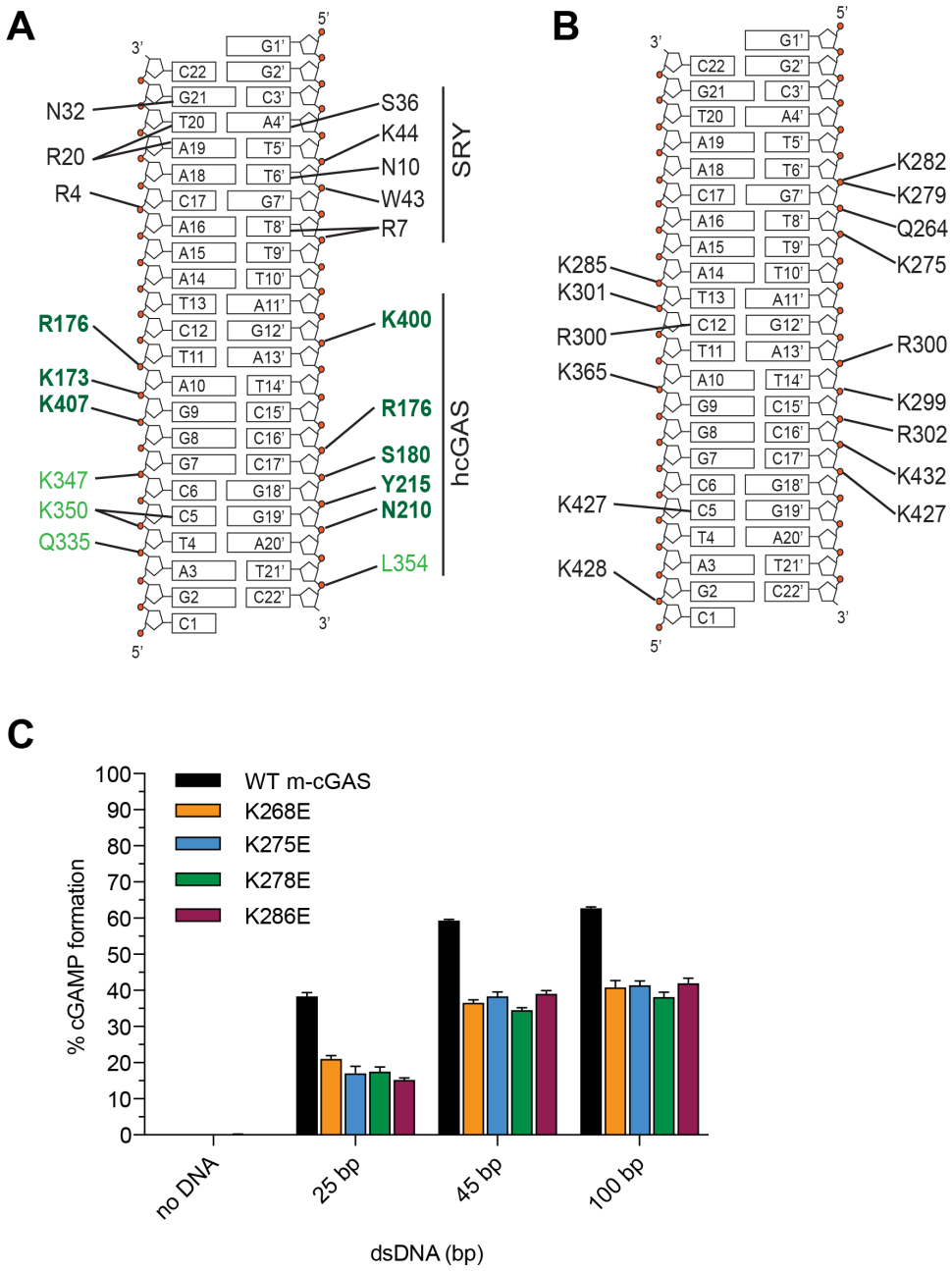

Fig. S2. Intermolecular contacts in dimeric SRY.h-cGAS^{CD}-DNA complex. (*A*) A schematic representation of the sequence-independent intermolecular site-A (dark green) and site-B (light green) contacts in the dimeric SRY.h-cGAS^{CD}-DNA complex. Also shown are the intermolecular contacts (black) between the SRY domain and its sequence-specific DNA target site in the complex. (*B*) A schematic representation of the sequence-independent intermolecular site-C (black) contacts in the dimeric SRY.h-cGAS^{CD}-DNA complex. (*C*) m-cGAS activities of mutations spanning site-C DNA binding surface, detected by RF-MS assay. For mouse cGAS, each reaction contains 300 nM DNA, 60 nM FL cGAS proteins, 300 μM ATP/GTP, incubated at 37˚C for 1h.

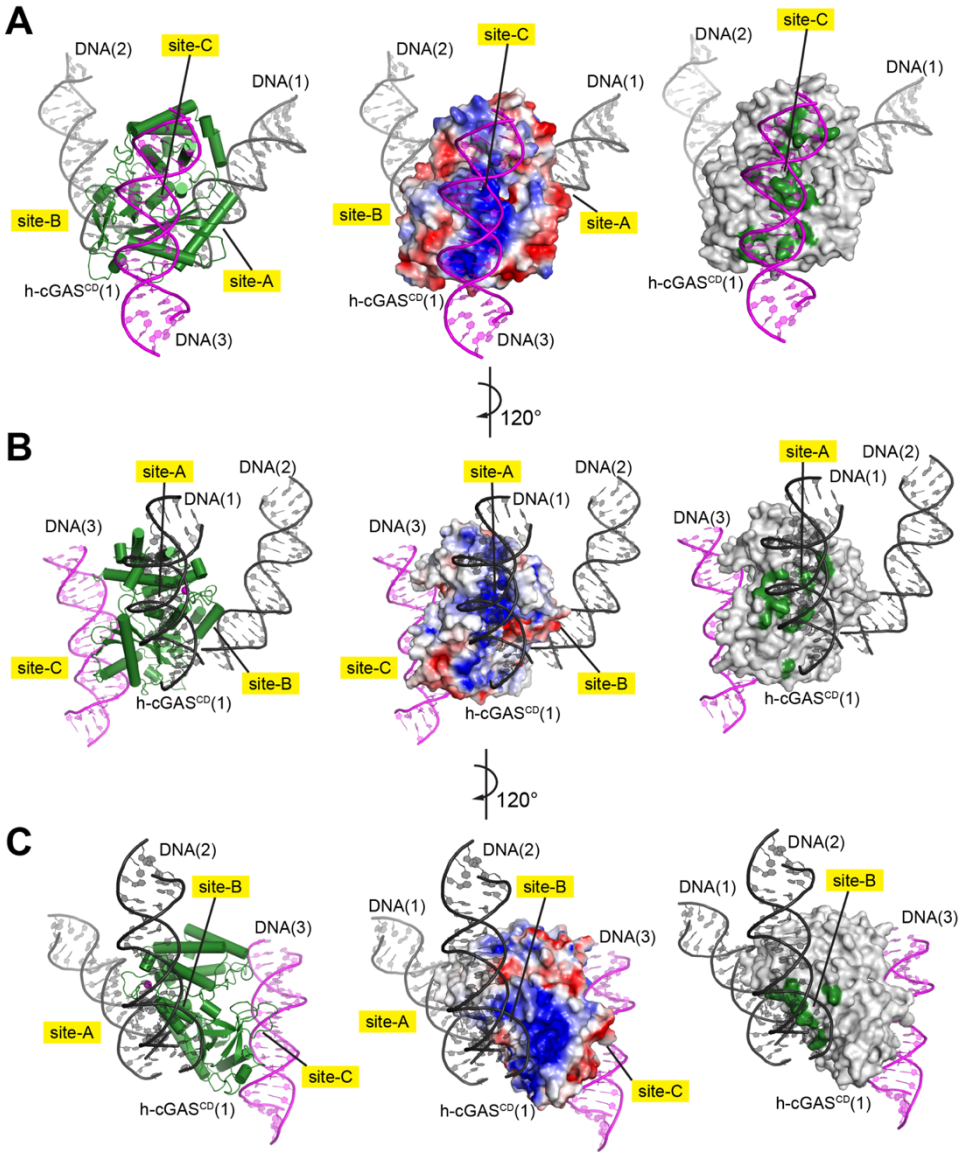

Fig. S3. Structural details of three DNA-binding surfaces of h-cGAS^{CD}. (*A*) The site-C interface observed between h-cGAS^{CD}(1) and DNA(3). (*B*) The site-A interface observed between h-cGAS^{CD}(1) and DNA(1). (*C*) The site-B interface observed between h-cGAS^{CD}(1) and DNA(2). The h-cGAS^{CD}(1) proteins are shown as ribbon (left panel), electrostatic surface potential (middle panel), and surface (right panel) representations. DNA(3) is colored in magenta, DNA (1) and DNA(2) are colored in black. Electrostatic surface potentials were calculated in PyMol and contoured at ±100. The interfaces are colored in green in surface representation. The positions of corresponding interfaces are indicated.

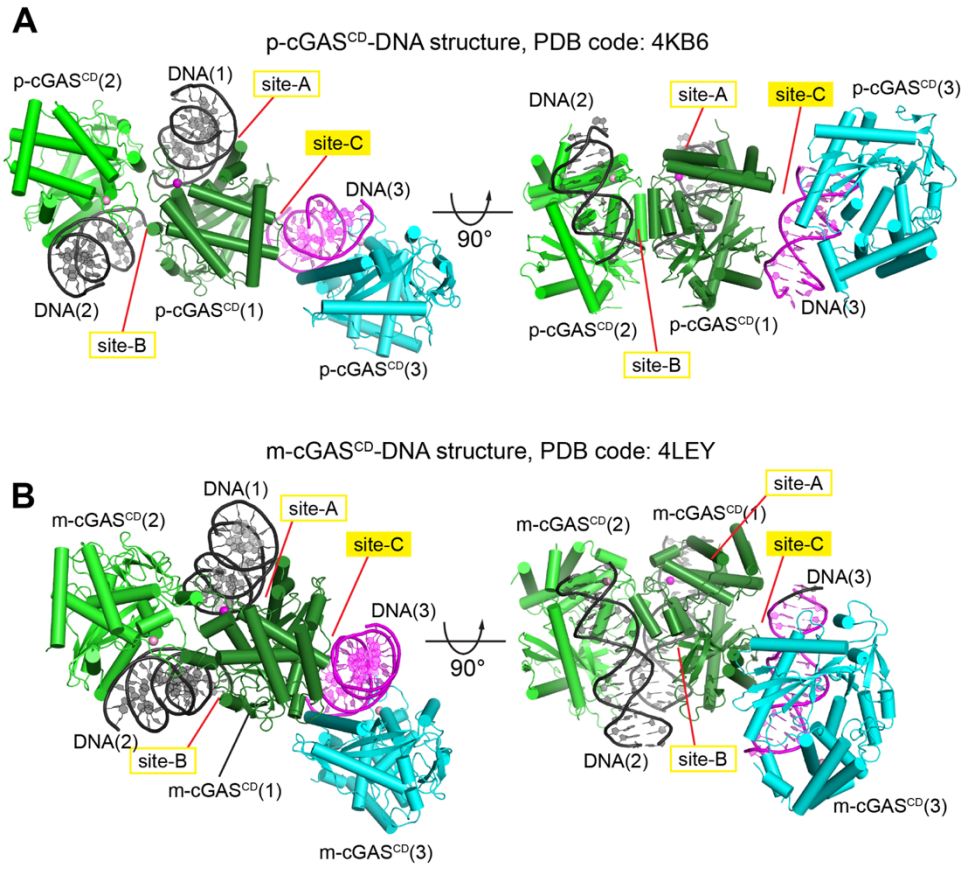

Fig. S4. Site-C interfaces are also observed in DNA-bound p-cGAS and m-cGAS structures. (*A*) Two views of crystal packing analysis of DNA-bound p-cGAS structure (PDB code: 4KB6) showing site-C interface between p-cGAS^{CD}(1) (in dark green) and DNA(3) (in magenta) associated with two adjacent asymmetric units. Site A, B and C are indicated by yellow boxes. (*B*) Two views of crystal packing analysis of DNA-bound m-cGAS structure (PDB code: 4LEY) showing site-C interface between m-cGAS^{CD}(1) (in dark green) and DNA(3) (in magenta) associated with two adjacent asymmetric units. Site A, B and C are indicated by yellow boxes.

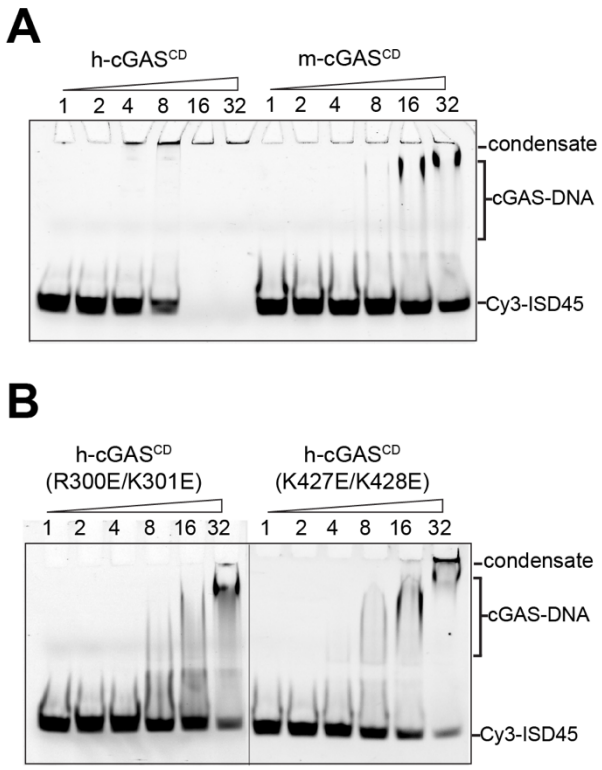

Fig. S5. Impact of the site-C interface mutations on DNA binding property of cGAS core domain as monitored by EMSA. (*A*) EMSA data for binding of Cy3-ISD45 to WT h-cGAS^{CD} and WT m-cGAS^{CD}. (*B*) EMSA data for binding of Cy3-ISD45 to h-cGAS^{CD} (R300E/K301E) and h-cGAS^{CD} (K427E/K428E). The molar ratio of cGAS to DNA is shown at the top of the gel. The cGAS-DNA condensate, the lower order of cGAS-DNA complex(es) and free Cy3-ISD45 are indicated on the right side of the 6% DNA retardation Gels. Data are representative of at least two independent experiments.

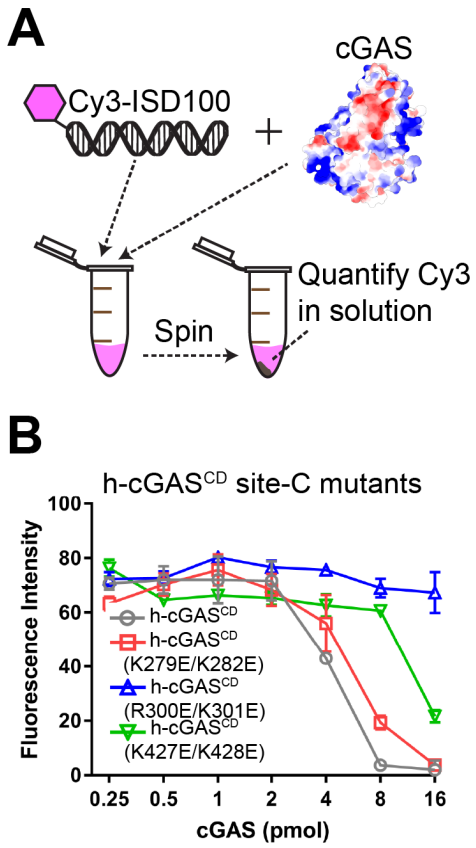

Fig. S6. Spin-down assay to monitor h-cGAS^{CD}-DNA condensation for site-C mutants. (*A*) Schematic of the DNA condensation assay used to quantify the partitioning of Cy3-labelled ISD100 into pellets and solution. (*B*) DNA condensation assay of Cy3-ISD100 with h-cGAS^{CD} proteins. 2-fold increasing concentrations of h-cGAS proteins (from 0.25 pmol to 16 pmol) were mixed with 1 pmol ISD100 for 1 h at room temperature. The fluorescence intensity values of Cy3 in the supernatant were plotted against cGAS protein concentrations. Data are represented as means ± SD of three independent experiments.

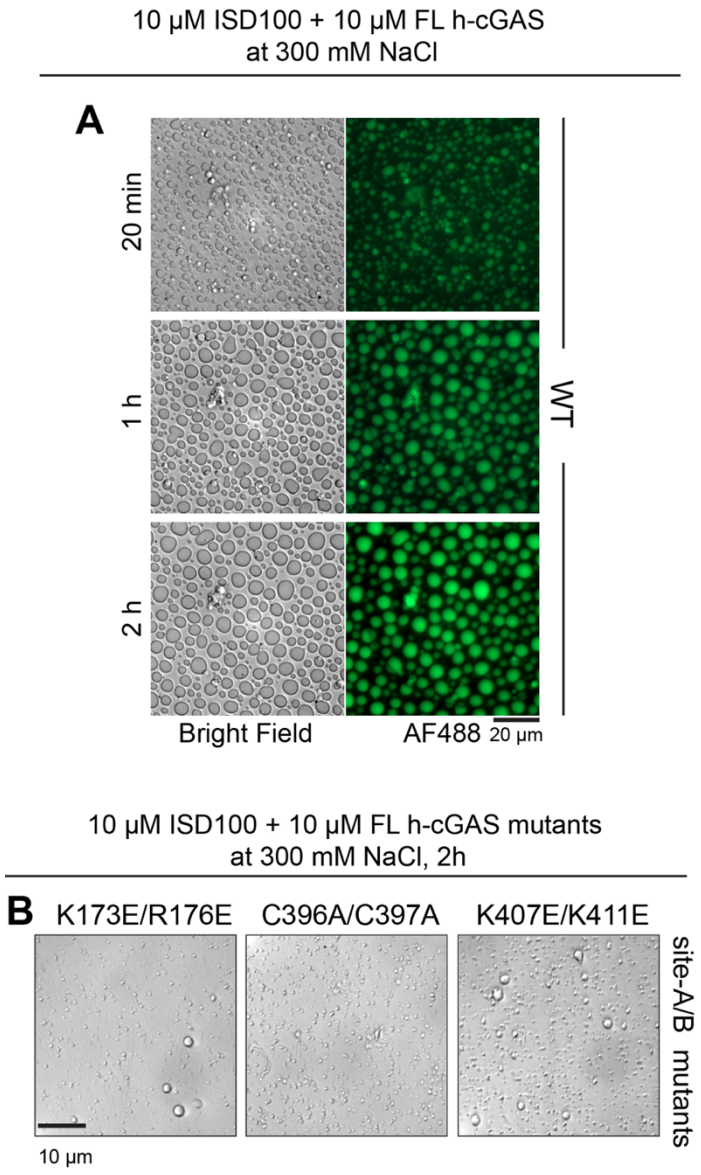

Fig. S7. The site-C DNA binding surface of cGAS is essential for DNA-induced phase separation as identified from time-lapse imaging of liquid droplet formation. (*A*) Time-lapse imaging of ISD100-induced FL h-cGAS phase separation. 10 μM FL h-cGAS (5% Alexa 488-labeled) was incubated with 10 μM 100-bp DNA and imaged from 20 min to 2 h by bright-field and GFP channels. The images shown are representative of all fields in the well. Scale bar, 20 μm. WT h-cGAS and 100-bp DNA formed micrometer-sized liquid droplets, which gradually fused into larger ones. (*B*) Bright-field imaging of liquid phase condensation data for FL h-cGAS site-A/B mutant (K173E/R176E, C396A/K397A, and K407E/K411E).

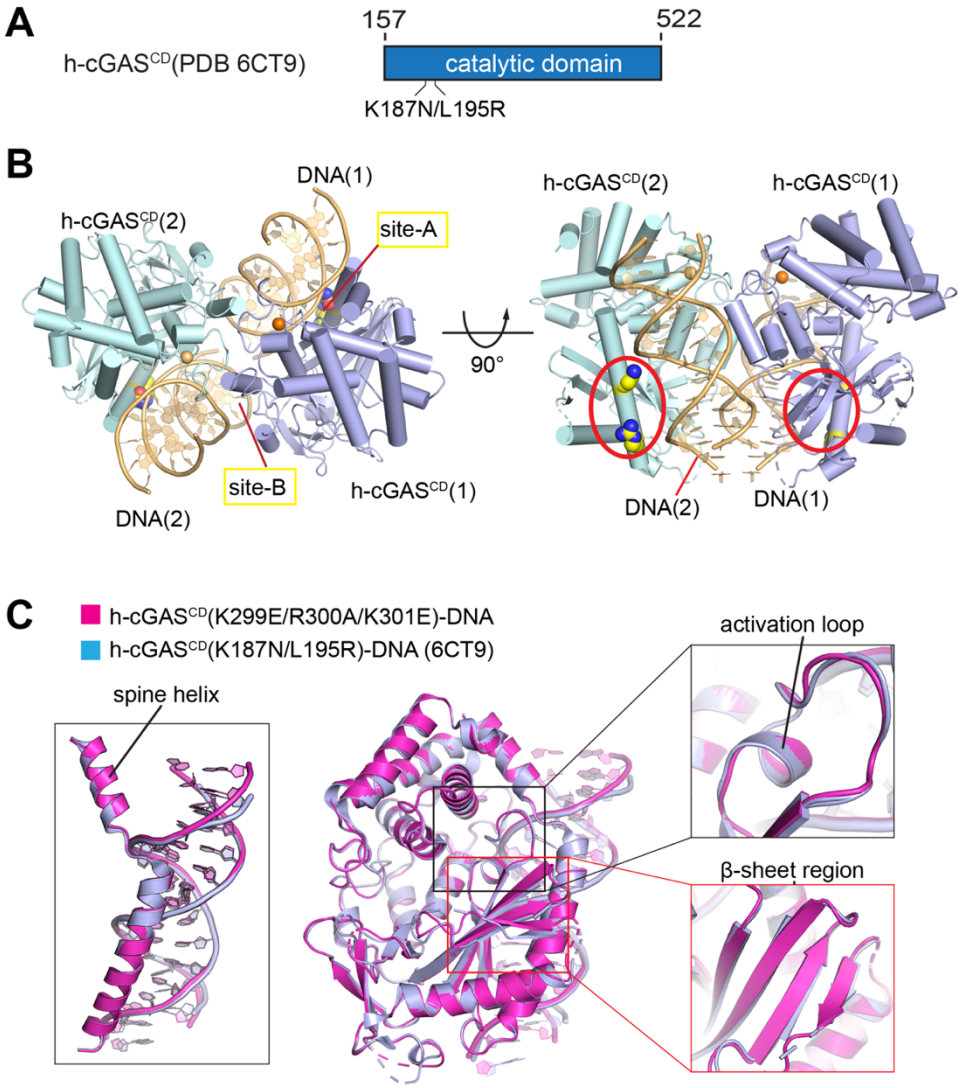

Fig. S8. Crystal Structure of h-cGAS^{CD} (K187N/L195R) bound to DNA and comparison with h-cGAS^{CD} (K299E/R300A/K301E) bound to DNA structure. (*A*) Schematic showing positioning of K187N/L195R dual mutant within h-cGAS^{CD}. (*B*) Side and top views of dimeric structure of h-cGAS^{CD} (K187N/L195R) bound to DNA (PDB: 6CT9). h-cGAS^{CD} monomers are colored in pale cyan and light blue while the pair of bound DNAs are colored in teal, with labeling of sites-A and site-B. The double mutation sites are shown in a space-filling representation and indicated by red circles. (*C*) Superposition of a pair of mutant dimeric SRY.h-cGAS^{CD}-DNA complexes. Superposed structures of DNA-bound h-cGAS^{CD} (K299E/R300A/K301E) (this study, in magenta) and h-cGAS^{CD} (K187N/L195R) (PDB: 6CT9, in light bule). The blow up views in a similar orientation indicate the degree of overlap amongst the α-helix spine, activation loop and β-sheet segments between the two structures, which exhibit good overlap with a r.m.s.d=0.286 Å.

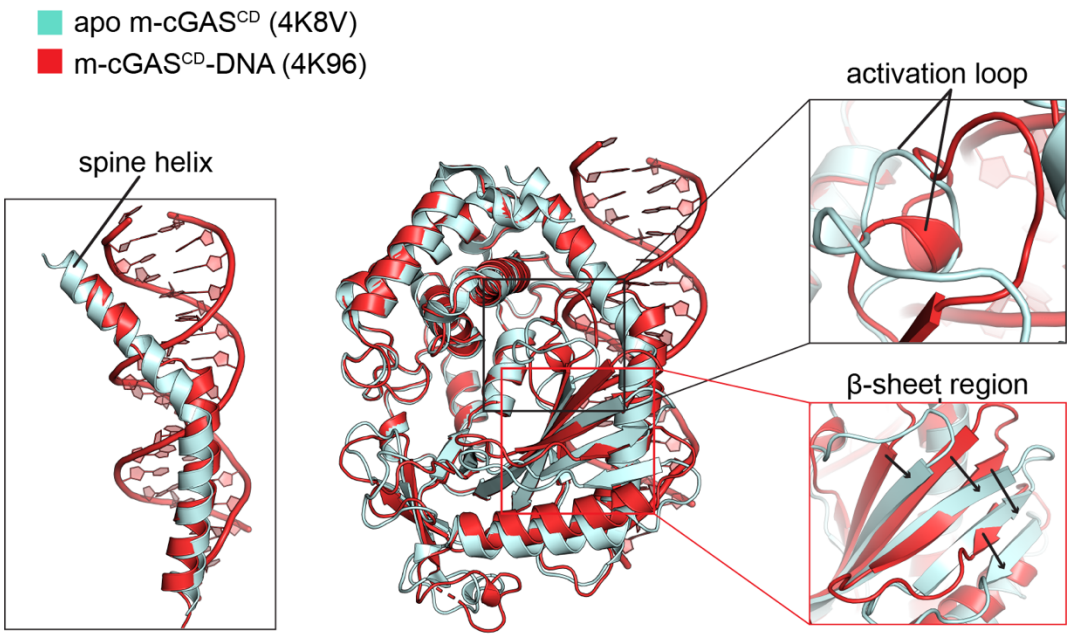

Fig. S9. Overlap between apo- and DNA-bound forms of m-cGAS^{CD}. Superposed structures of apo m-cGAS^{CD} (PDB: 4K8V; in light cyan) and DNA-bound m-cGAS^{CD} (PDB: 4K96; in red). The structures of the two complexes exhibit an r.m.s.d = 0.614 Å. The blow up views in compare conformational changes of the α-helix spine (left panel), activation loop (upper right panel) and β-sheet segments (lower right panel). Black arrows indicate the large shift in β-strands on proceeding from apo- to DNA-bound states.

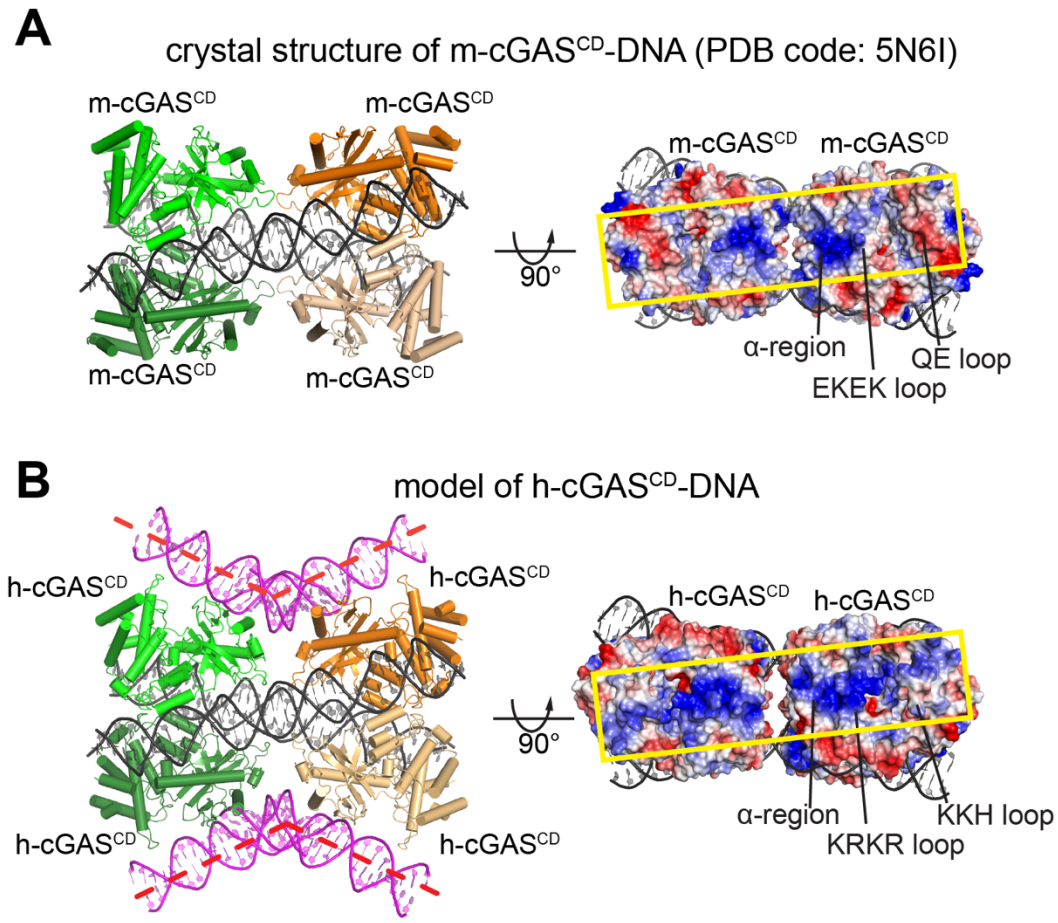

Fig. S10. Crystal structure of m-cGAS^{CD}-DNA and a model of h-cGAS-DNA with implications for condensation and phase separation. (*A*) Crystal structure in the left panel of the complex of a pair of m-cGAS^{CD} dimers (in green and orange) bound to a pair of 39-bp DNAs (in black) (PDB code: 5N6I). Electrostatic surface potential representation of the complex is shown in the right panel, with the pair of m-cGAS^{CD} dimers exhibiting an extended pair of site-C DNA interfaces (highlighted by yellow box). Electrostatic surface potential was calculated by PyMol and contoured at ± 100. (*B*) Model in the left panel of h-cGAS^{CD} dimers bound to long DNA was generated by superimposing dimeric SRY.h-cGAS^{CD}-DNA complex (SRY domains not shown; only 21-bp DNAs bound at site-C are shown) with the dimeric m-cGAS^{CD}-39bp DNA structure (PDB code: 5N6I). The pair of h-cGAS^{CD} dimers are colored green and orange, the 39-bp DNAs are colored black and the 21-bp DNAs are colored magenta. Electrostatic surface potential representation of the model is shown in the right panel, which reveals an extended pair of site-C DNA interfaces (highlighted by yellow box). Electrostatic surface potential was calculated by PyMol and contoured at ± 100.

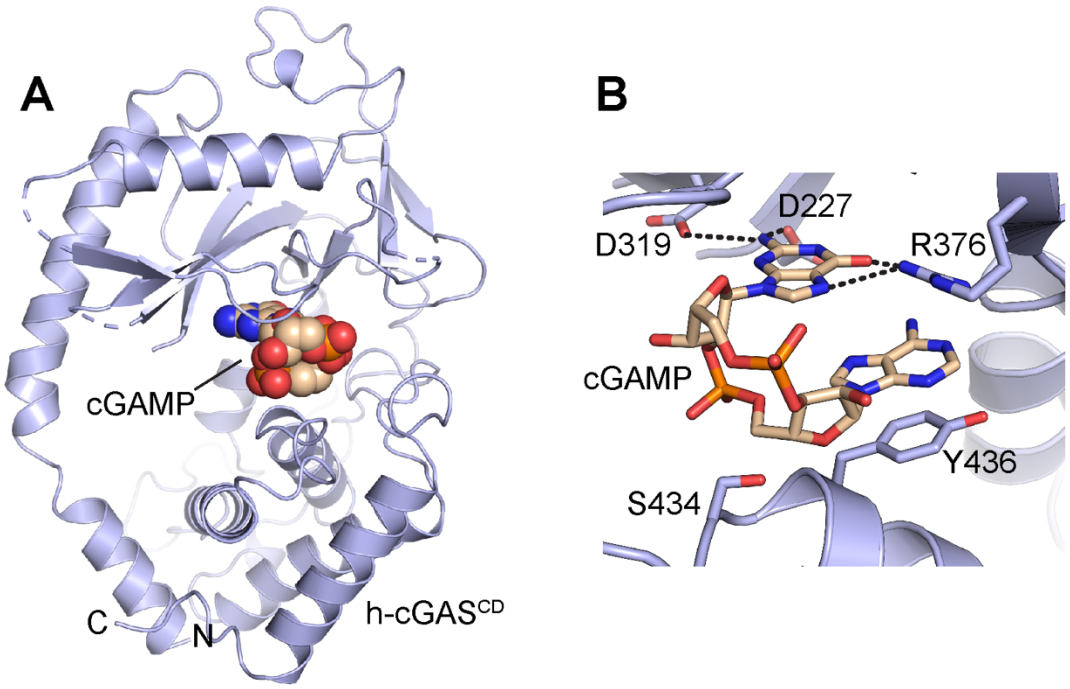

Fig. S11. Structure of 2′,3′-cGAMP bound to apo h-cGAS^{CD}. (*A*) Crystal structure of cGAMP bound to apo h-cGAS^{CD}(K427E/K428E)(PDB code: 6MJX). The h-cGAS^{CD} is shown in light blue cartoon. The bound cGAMP positioned in the catalytic pocket is shown in a space-filling representation. (*B*) Detailed interactions between cGAMP and h-cGAS^{CD}. The residues contributing to the interaction is shown in light blue sticks. The bound cGAMP is shown in wheat sticks. The hydrogen bonds are shown in black dash lines.

Table S1. X-ray statistics

	SRY.hcGAS^{CD}-DNA **(PDB 6EDB)**	***hcGAS^{CD}-DNA*** **(PDB 6EDC)**	***hcGAS^{CD}-RU.521*** **(PDB 6O47)**
Data collection			
Wavelength (Å)	0.9792	0.9792	0.9792
Space group	*I*222	$P6_122$	$P6_4$
Cell dimensions			
a, b, c (Å)	90.3, 115.8, 159.0	99.8, 99.8, 238.6	116.2, 116.2, 60.0
α, β, γ (°)	90, 90, 90	90, 90,120	90, 90, 120
Resolution (Å)	30.01-3.20 (3.32-3.20)	86.44-2.71 (2.80-2.71)	29.27-2.20 (2.28-2.20)
R-pim (%)	5.1 (33.8)	6.2 (69.1)	2.5 (23.9)
I/σI	13.4 (1.6)	11.3 (1.0)	33.9 (4.0)
Completeness (%)	90.3 (61.6)	98.4 (96.1)	99.7 (98.1)
Redundancy	5.4 (3.5)	12.0 (10.8)	10.5 (7.0)
CC1/2	0.980 (0.722)	0.996 (0.506)	0.926 (0.849)
Refinement			
R_{work}/R_{free} *(%)*	25.5/30.2	23.9/27.7	18.1/22.1
No. of non-hydrogen atoms			
Protein/DNA	4378	3499	2854
Ligand/Ion	1	1	83
Water	0	0	180
B-factors (Å^2)			
Protein/DNA	105.4	67.8	41.88
Ligand/Ion	30.0	81.0	42.21
Water	0	0	41.15
R.m.s. deviations			
Bond lengths (Å)	0.004	0.003	0.006
Bond angles (°)	0.82	0.51	1.02
Ramachandran plots			

Favored (%)	92.4	94.9	96.7
Allowed (%)	7.4	5.1	3.0
Outliers (%)	0.2	0	0.3
Statistics for the highest-resolution shell are shown in parenthesis.			